



HAL
open science

A micromechanical model of a hard interface with micro-cracking damage

Maria Letizia Raffa, Frédéric Lebon, Raffaella Rizzoni

► **To cite this version:**

Maria Letizia Raffa, Frédéric Lebon, Raffaella Rizzoni. A micromechanical model of a hard interface with micro-cracking damage. *International Journal of Mechanical Sciences*, 2022, 216, pp.106974. 10.1016/j.ijmecsci.2021.106974 . hal-03404654

HAL Id: hal-03404654

<https://hal.science/hal-03404654>

Submitted on 26 Oct 2021

HAL is a multi-disciplinary open access archive for the deposit and dissemination of scientific research documents, whether they are published or not. The documents may come from teaching and research institutions in France or abroad, or from public or private research centers.

L'archive ouverte pluridisciplinaire **HAL**, est destinée au dépôt et à la diffusion de documents scientifiques de niveau recherche, publiés ou non, émanant des établissements d'enseignement et de recherche français ou étrangers, des laboratoires publics ou privés.

A micromechanical model of a hard interface with micro-cracking damage

Maria Letizia Raffa^{a,*}, Frédéric Lebon^b, Raffaella Rizzoni^c

^a*Laboratoire QUARTZ, EA 7393, ISAE-Supméca, 3 rue Fernand Henriod 93407 Saint-Ouen, France*

^b*Aix Marseille Univ, CNRS, Centrale Marseille, LMA, 4 impasse Vivier, Tota 13453 Marseille Cedex 13, France*

^c*Department of Engineering, University of Ferrara, via Saragat 1 44122 Ferrara, Italy*

Abstract

Bonding techniques are increasingly used in many industrial fields. Modelling the under-load damaging behavior of hard structural adhesives is still an open challenge. This work proposes a new hard interface analytical model with evolutive micro-cracking damage. The model is obtained within a rigorous theoretical framework combining asymptotic theory and micromechanical homogenization. Main new features are: (i) the adoption of two dual homogenization approaches; (ii) the formulation of a thermodynamically-based damage evolution law for hard interfaces. The interface model is able to describe both ductile and brittle damage behavior of hard structural adhesives. Provided examples on the structural behavior, under several loads, suggest the suitability of the proposed interface model as a modelling strategy for hard structural adhesives with micro-cracking damage.

*Corresponding author

Email addresses: maria-letizia.raffa@isae-supmeca.fr (Maria Letizia Raffa), lebon@lma.cnrs-m.fr (Frédéric Lebon), raffaella.rizzoni@unife.it (Raffaella Rizzoni)

Keywords: bonding, adhesives, damage, imperfect interfaces,
homogenization, asymptotic theory

1. Introduction

Bonding has become a very common practice to assembly materials and structural elements in many industrial fields, such as aeronautic spatial, automotive, nuclear, civil, mechanical and bio-engineering mainly because structural adhesives offer low-cost techniques and a great design freedom while preserving good mechanical performances. For some applications, such as assemblies of fiber-reinforced composites and implant fixations, bonding is the only viable assembly technology. To achieve better performances avoiding too large mismatch in terms of thermo-elastic properties, structural adhesives and adherents have, in some cases, an equivalent stiffness. Some examples can be cited: acrylic adhesives, whose Young's modulus (E) is around 2-3 GPa [1], are used in manufacture of plywood ($E = 5 - 8$ GPa); phenolic and epoxy adhesives with $E = 3 - 5$ GPa [2] are used to bond structures of GFRP (polyester-glass composites) with $E = 15 - 28$ GPa; orthodontic adhesives with $E = 18 - 22$ GPa [3] are usually used for cementation of brackets on enamel ($E \simeq 65$ GPa).

An adhesive equally stiffer than adherents is defined, from a mechanical point of view, as a *hard* interface, as opposed to the definition of *soft* interface [4, 5]. A wide literature exists concerning models of soft material interfaces, including those undergoing material degradation. Analytical soft interface models often take into account the nonlinear evolution of the interface properties by introducing at least one parameter (of damage, adhesion,

etc.) whose variation depends macroscopically on kinematic variables [6–15]. Numerical soft interface models, in the framework of the finite element theory, generally use cohesive zone models (CZM) based on traction-separation laws of various shapes, to describe cohesive and adhesive failure [16–22].

Recently, some analytical models of hard material interfaces have been also developed [23–29] and it has been proved that interface models developed for soft adhesives cannot be directly applied in the case of hard adhesives [25]. Moreover, the existing hard interface models do not consider the degradation of the adhesive material properties.

This paper provides a novelty within this context, by proposing a hard material interface model accounting for an evolving micro-cracking damage. In the last twenty years, the present authors established an original modelling strategy to derive soft and hard imperfect interface models based on the combination of asymptotic theory and micromechanical homogenization [11, 14, 23–26] (see Fig. 1). This strategy has already been successfully used to describe the mechanics of thin elastic layers in adhesive-like problems and contact problems [13, 15, 30, 31]. Moreover, it has been identified as a sound alternative to the classical cohesive zone models, principally because imperfect interface models allow to consider the physics of the adhesives in terms of geometrical (thickness, surface roughness), mechanical (anisotropy, non-linearity) and damage properties.

This work is an extension of the authors’ modelling strategy of hard imperfect interfaces. Drawing on Kachanov’s micromechanical homogenization theory [32–37], micro-cracking damage is represented by a microcracks density parameter. Particularly, the adoption of a generalized cracks density [38]

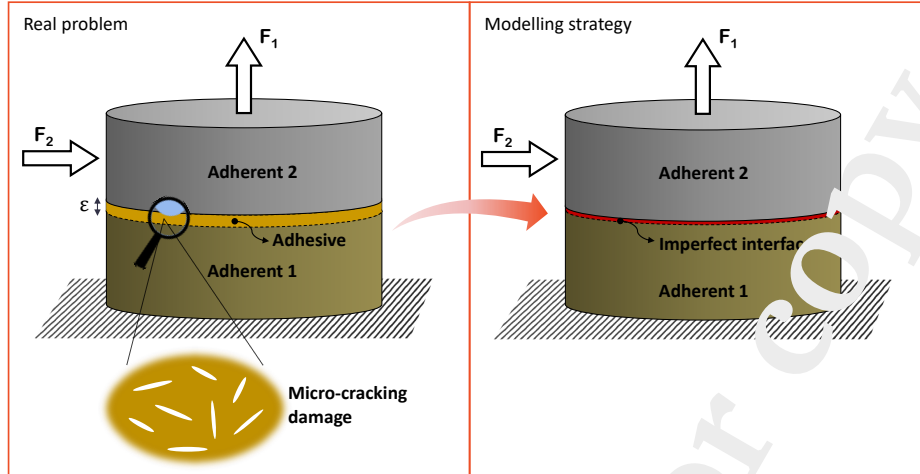


Fig. 1: Schematic sketch of the imperfect interface modelling strategy

48 allows to by-pass the geometrical definition of the cracks, which is possible
 49 only for circular and regular cracks [32], and as a matter of fact it extends the
 50 generality of the proposed interface model to any regular and irregular cracks
 51 shape. It should also be noted that the generalized microcracks density can
 52 be measured *postmortem* by X-ray micro-tomography [15]. The evolutive
 53 character of the micro-cracking damage is described by introducing a new
 54 evolution law of the generalized cracks density.

55 The paper is structured as follows. The hard imperfect interface law is
 56 derived via the asymptotic expansions method in Section 2. In Section 3,
 57 the microcracked-material-interface properties are derived through two dual
 58 approaches of micromechanical homogenization, stress [32, 33] and strain-
 59 based [39, 40]. The damage evolution law is derived from a thermodynamic

60 approach and then included in the hard interface model via the asymptotic
61 expansions method. In Section 4, the behavior of the proposed interface
62 model under various loading type is discussed via some academic examples.
63 Moreover, the influence of damage parameters is investigated. Conclusions
64 and perspectives are drawn at the end of the paper.

65 **2. Derivation of the hard imperfect interface model**

66 *2.1. Notation and problem statement*

67 The herein adopted matched asymptotic expansion theory builds on the
68 tradition of using asymptotic analysis to derive mechanical laws governing
69 imperfect interface conditions [41–48].

70 In what follows, a thin material layer of constant thickness t embedded
71 between at least two solids is referred as *interphase*. Being L a representa-
72 tive length scale of the geometry, the non-dimensional interphase thickness
73 $\varepsilon = t/L$ can be defined and taken as a small parameter for the asymptotic
74 expansions of the elastic problem. When $\varepsilon \ll 1$, the thin layer can be sub-
75 stituted by a surface separating the adherents called *interface* across which
76 certain conditions on the displacements and tractions prevail [4].

77 The interphase occupies a domain \mathcal{B}^ε with cross-section \mathcal{S} , \mathcal{S} being an
78 open bounded set in \mathbb{R}^2 with smooth boundary. The *adherents* occupy the
79 reference configurations $\Omega_\pm^\varepsilon \subset \mathbb{R}^3$. Let $\mathcal{S}^\varepsilon_\pm$ be taken to denote the plane
80 interfaces between interphase and adherents and let $\Omega^\varepsilon = \Omega_\pm^\varepsilon \cup \mathcal{S}^\varepsilon_\pm \cup \mathcal{B}^\varepsilon$
81 denote the whole composite system. It is assumed that the displacement and
82 stress vector fields are continuous across $\mathcal{S}^\varepsilon_\pm$.

83 An orthonormal Cartesian basis $(O, \mathbf{i}_1, \mathbf{i}_2, \mathbf{i}_3)$ is introduced and let (x_1, x_2, x_3)

84 be taken to denote the three coordinates of a particle. The origin of the basis
 85 belongs to \mathcal{S} . The aforementioned system is sketched in Fig. 2a.

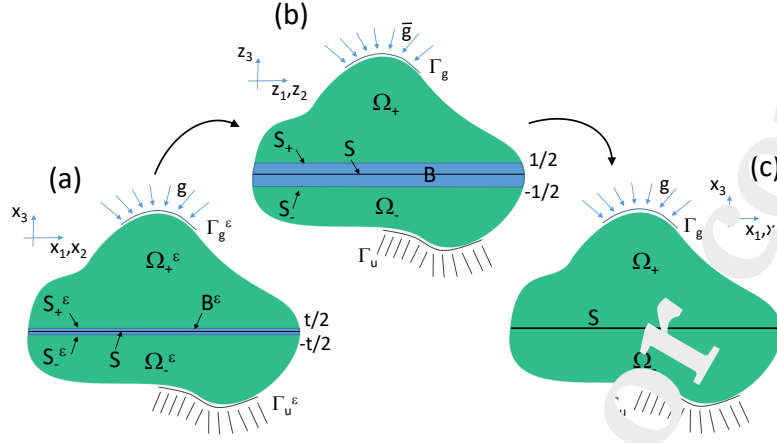


Fig. 2: The three steps of the matched asymptotic expansion method: (a) Reference configuration (interphase); (b) Rescaled configuration (asymptotic expansion phase); (c) Limit configuration (interface).

86 The materials of the composite system are assumed to be homogeneous
 87 and linearly elastic and let $\mathbb{A}_\pm, \mathbb{B}^\epsilon$ be the fourth-rank elasticity tensors of
 88 adherents and of interphase, respectively. Tensors $\mathbb{A}_\pm, \mathbb{B}^\epsilon$ have the usual
 89 symmetry properties, with the minor and major symmetries, and are posi-
 90 tive definite. Note that an assumption on the anisotropy of adhesive and
 91 adherents materials is needed for the proposed development. As a matter of
 92 fact, it extends the generality of the proposed asymptotic approach to any
 93 anisotropic material.

94 Adherents are subjected to a body force density $\mathbf{f}^\pm : \Omega^\epsilon_\pm \mapsto \mathbb{R}^3$ and to a
 95 surface force density $\mathbf{g}^\pm : \Gamma_g^\epsilon \mapsto \mathbb{R}^3$ on $\Gamma_g^\epsilon \subset (\partial\Omega^\epsilon_+ \setminus \mathcal{S}_+^\epsilon) \cup (\partial\Omega^\epsilon_- \setminus \mathcal{S}_-^\epsilon)$. Body

96 forces in the interphase are neglected.

97 On $\Gamma_u^\varepsilon = (\partial\Omega^\varepsilon_+ \setminus \mathcal{S}_+^\varepsilon) \cup (\partial\Omega^\varepsilon_- \setminus \mathcal{S}_-^\varepsilon) \setminus \Gamma_g^\varepsilon$, homogeneous boundary conditions
98 are prescribed:

$$\mathbf{u}^\varepsilon = \mathbf{0} \quad \text{on } \Gamma_u^\varepsilon, \quad (1)$$

99 where $\mathbf{u}^\varepsilon : \Omega^\varepsilon \mapsto \mathbb{R}^3$ is the displacement field defined on Ω^ε . Boundaries
100 Γ_g^ε , Γ_u^ε are assumed to be located sufficiently far from the interphase and the
101 external boundaries of the interphase \mathcal{B}^ε ($\partial\mathcal{S} \times (-\frac{\varepsilon}{2}, \frac{\varepsilon}{2})$) are assumed to be
102 stress-free. The external forces field is endowed with sufficient regularity to
103 ensure the existence of an equilibrium configuration [25].

104 The following notation is adopted:

- 105 • $[f] := f(\mathbf{z}_\alpha, \frac{1}{2}) - f(\mathbf{z}_\alpha, -\frac{1}{2}) \Rightarrow$ jump in the rescaled configuration (Fig. 2b);
- 106 • $\langle f \rangle := \int_{-\frac{1}{2}}^{\frac{1}{2}} f(\mathbf{z}_\alpha, z_3) dz_3 \Rightarrow$ average in the rescaled configuration;
- 107 • $[[f]] := f(\mathbf{x}_\alpha, 0^+) - f(\mathbf{x}_\alpha, 0^-) \Rightarrow$ jump in the limit configuration (Fig. 2c);
- 108 • $\langle\langle f \rangle\rangle := \frac{1}{2}(f(\mathbf{x}_\alpha, 0^+) + f(\mathbf{x}_\alpha, 0^-)) \Rightarrow$ average in the limit configuration;

109 where f is a generic function, $\mathbf{z}_\alpha = (z_1, z_2)$ and $\mathbf{x}_\alpha = (x_1, x_2)$.

110 2.2. The one-order asymptotic theory

111 This section details the main steps of the asymptotic analysis leading to
112 the hard interface law at one order. Full formulation is reported in Appendix
113 A and more details could be found in [23–26].

114 Generally, the elasticity tensor \mathbb{B}^ε of a hard interphase does not depend
115 on ε [23, 25]:

$$\mathbb{B}^\varepsilon = \mathbb{B} \quad (2)$$

116 In the rescaled configuration (Fig. 2b) and considering Eqs. (A.7) and
 117 (A.14b), the stress-strain equation (A.31b) reads as:

$$\hat{\boldsymbol{\sigma}}^0 + \varepsilon \hat{\boldsymbol{\sigma}}^1 = \mathbb{B}(\varepsilon^{-1} \hat{\mathbf{e}}^{-1} + \hat{\mathbf{e}}^0 + \varepsilon \hat{\mathbf{e}}^1) + o(\varepsilon) \quad (3)$$

Equation (3) is true $\forall \varepsilon$, thus the following conditions are derived:

$$\mathbf{0} = \mathbb{B}(\hat{\mathbf{e}}^{-1}) \quad (4a)$$

$$\hat{\boldsymbol{\sigma}}^0 = \mathbb{B}(\hat{\mathbf{e}}^0) \quad (4b)$$

118 By considering Eq. (A.8) and the positive definiteness of the tensor \mathbb{B} , Eq. (4a)
 119 gives:

$$\hat{\mathbf{u}}_{,3}^0 = 0 \Rightarrow [\hat{\mathbf{u}}^0] = \mathbf{0} \quad (5)$$

120 Moreover, substituting Eq. (A.9) written for $k = j$ into Eq. (4b) it gives:

$$\hat{\boldsymbol{\sigma}}^0 \mathbf{i}_j = \mathbf{K}^{1j} \hat{\mathbf{u}}_{,1}^0 + \mathbf{K}^{2j} \hat{\mathbf{u}}_{,2}^0 + \mathbf{K}^{3j} \hat{\mathbf{u}}_{,3}^1 \quad (6)$$

121 with $j = 1, 2, 3$ and \mathbf{K}^{jl} being the two-order tensors such that $K_{ki}^{jl} := B_{ijkl}$.

122 Next, integrating Eq. (6) with respect to z_3 (for $j = 3$) and considering

123 Eq. (A.17) it results:

$$[\hat{\mathbf{u}}^1] = (\mathbf{K}^{33})^{-1} (\mathcal{J}^0 \mathbf{i}_3 - \mathbf{K}^{\alpha 3} \hat{\mathbf{u}}_{,\alpha}^0) \quad (7)$$

124 Then, by replacing Eq. (6) ($j = 1, 2$) in the equilibrium equation (A.18) one

125 obtains:

$$(\hat{\boldsymbol{\sigma}}^1 \mathbf{i}_3)_{,3} = -(\mathcal{J}^1 \mathbf{i}_\alpha)_{,\alpha} = -(\mathbf{K}^{1\alpha} \hat{\mathbf{u}}_{,1}^0 + \mathbf{K}^{2\alpha} \hat{\mathbf{u}}_{,2}^0 + \mathbf{K}^{3\alpha} \hat{\mathbf{u}}_{,3}^1)_{,\alpha} \quad (8)$$

126 Next, by integrating Eq. (8) with respect to z_3 between $-1/2$ and $1/2$ and

127 by using Eq. (7) it is obtained:

$$[\hat{\boldsymbol{\sigma}}^1 \mathbf{i}_3] = \left(-\mathbf{K}^{\beta\alpha} \hat{\mathbf{u}}_{,\beta}^0 - \mathbf{K}^{3\alpha} (\mathbf{K}^{33})^{-1} (\hat{\boldsymbol{\sigma}}^0 \mathbf{i}_3 - \mathbf{K}^{\beta 3} \hat{\mathbf{u}}_{,\beta}^0) \right)_{,\alpha} \quad (9)$$

128 where Greek indexes ($\alpha, \beta = 1, 2$) are related to the in-plane (x_1, x_2) quan-
 129 tities. Note that in Eq. (9) higher order effects, related to in-plane deriva-
 130 tives, appear. These terms, usually neglected in standard zero-order theories
 131 [23, 25], are related to the curvature of the deformed interface (second-order
 132 derivatives).

133 Finally, the transition from the rescaled configuration to the initial configura-
 134 tion is obtained by introducing the matching conditions Eq.(A.27)-(A.30)
 135 and the interface laws at both zero-order and one-order are derived:

- Zero-order interface law:

$$[[\mathbf{u}^0]] = \mathbf{0} \quad (10)$$

$$[[\boldsymbol{\sigma}^0 \mathbf{i}_3]] = \mathbf{0} \quad (11)$$

- One-order interface law:

$$[[\mathbf{u}^1]] = (\mathbf{K}^{33})^{-1} (\boldsymbol{\sigma}^0 \mathbf{i}_3 - \mathbf{K}^{\alpha 3} \mathbf{u}_{,\alpha}^0) - \langle\langle \mathbf{u}_{,3}^0 \rangle\rangle \quad (12)$$

$$[[\boldsymbol{\sigma}^1 \mathbf{i}_3]] = \left(-\mathbf{K}^{\beta \alpha} \mathbf{u}_{,\beta}^0 - \mathbf{K}^{\alpha 3} (\mathbf{K}^{33})^{-1} (\boldsymbol{\sigma}^0 \mathbf{i}_3 - \mathbf{K}^{\beta 3} \mathbf{u}_{,\beta}^0) \right)_{,\alpha} \\ - \langle\langle \boldsymbol{\sigma}_{3,3}^0 \mathbf{i}_3 \rangle\rangle \quad (13)$$

136 Equations (10)-(11) are the standard perfect interface condition, character-
 137 ized by the continuity in terms of displacements and stresses at the interface
 138 [4]. Equations (12)-(13) are the displacements and stresses jumps at the inter-
 139 face in the one-order asymptotic theory. They depend on the displacements
 140 and the stresses fields at the zero-order and on their first and second-order
 141 derivatives.

142 The hard interface law in the reference configuration (Fig.2a) is derived by
 143 considering asymptotic expansions (A.14a) and (A.5a) combined with Eqs.
 144 (10)-(13) [25]:

$$[[\mathbf{u}^\varepsilon]] \approx \varepsilon \left((\mathbf{K}^{33})^{-1} (\langle\langle \boldsymbol{\sigma}^\varepsilon \mathbf{i}_3 \rangle\rangle - \mathbf{K}^{\alpha 3} \langle\langle \mathbf{u}_{,\alpha}^\varepsilon \rangle\rangle) - \langle\langle \mathbf{u}_{,3}^\varepsilon \rangle\rangle \right) \quad (14)$$

$$[[\boldsymbol{\sigma}^\varepsilon \mathbf{i}_3]] \approx \varepsilon \left(\left(-\mathbf{K}^{\beta \alpha} \langle\langle \mathbf{u}_{,\beta}^\varepsilon \rangle\rangle - \mathbf{K}^{3\alpha} (\mathbf{K}^{33})^{-1} (\langle\langle \boldsymbol{\sigma}^\varepsilon \mathbf{i}_3 \rangle\rangle - \mathbf{K}^{\beta 3} \langle\langle \mathbf{u}_{,\beta}^\varepsilon \rangle\rangle) \right)_{,\alpha} \right. \\ \left. - \langle\langle \boldsymbol{\sigma}_{,3}^\varepsilon \mathbf{i}_3 \rangle\rangle \right) \quad (15)$$

145 3. Introduction of the micro-cracking damage

146 In this section, it is shown how to include micro cracking damage in the
 147 hard interface law above obtained. The closed-form of the effective elastic
 148 tensors \mathbf{K}^{jl} in Eqs. (14)-(15) is specialized by using micromechanical ho-
 149 mogenization in the case of two microcracked material models: Kachanov-
 150 Sevostianov (KS) and Welemane-Goidescu (WGC) models. The evolution law
 151 of the generalized microcracks density is derived from a thermodynamic ap-
 152 proach and then included in the hard interface model via the asymptotic
 153 expansions method.

154 3.1. Micromechanical homogenization approaches

155 The Kachanov-Sevostianov model [32, 37] is a stress-based approach based
 156 on the non-interacting microcracks approximation [35, 36]. The Welemane-
 157 Goidescu model [40, 49, 50] is a strain-based approach, based on the dilute
 158 limit hypothesis [39]. For both models, it is assumed that the material in-
 159 terphase comprises an orthotropic matrix embedding a family of microcracks
 160 parallel to \mathbf{i}_1 . For the sake of simplicity, the formulations are reduced to

161 the two-dimensional case on the plane $(\mathbf{i}_1, \mathbf{i}_3)$ with reference to the problem
 162 geometry in Fig.2.

163 3.1.1. Kachanov-Sevostianov model

164 Following the theory proposed by Kachanov and coworkers [32, 33] based
 165 on the Eshelby's approach [51], and the above assumptions on microcracks
 166 and matrix, the interface stiffness can be derived as follows:

$$\begin{aligned}
 K_{11}^{11} &= \frac{(E_1^0)^2 (2 R B_{nn} E_3^0 + 1)}{E_1^0 - E_3^0 (\nu_{13}^0)^2 + 2 R B_{nn} E_1^0 E_3^0} \\
 K_{31}^{13} &= K_{13}^{31} = \frac{E_1^0 E_3^0 \nu_{13}^0}{E_1^0 - E_3^0 (\nu_{13}^0)^2 + 2 R B_{nn} E_1^0 E_3^0} \\
 K_{33}^{33} &= \frac{E_1^0 E_3^0}{E_1^0 - E_3^0 (\nu_{13}^0)^2 + 2 R B_{nn} E_1^0 E_3^0} \\
 K_{11}^{33} &= \frac{2 G_{13}^0}{2 + R B_{tt} G_{13}^0}
 \end{aligned} \tag{16}$$

167 where E_1^0 , E_3^0 , G_{13}^0 , ν_{13}^0 and ν_{31}^0 are the in-plane elastic orthotropic moduli of
 168 the matrix; B_{nn} and B_{tt} are elastic parameters depending on the matrix and
 169 microcracks characteristics [32, 33].

170 Note that the engineering modulus can be also easily derived. The effective
 171 Young's modulus in normal direction (\mathbf{i}_3) , used in the examples below, reads
 172 as:

$$E_{\text{eff}} = \frac{E_3^0}{1 + 2 R B_{nn} E_3^0} \tag{17}$$

173 3.1.2. Welemane-Goide's model

174 In [40, 49, 50, 52], Welemane and coworkers extended the energy-based
 175 homogenization approach originally proposed in [39] for isotropic materials
 176 to the case of an orthotropic matrix.

177 By following the Welemane-Goidescu model [49], the expressions of the
 178 interface stiffness read as:

$$\begin{aligned}
 K_{11}^{11} &= \frac{E_1^0}{E_3^0(\nu_{13}^0\nu_{31}^0 - 1)^2} \left(E_3^0(1 - \nu_{13}^0\nu_{31}^0) - R\sqrt{E_3^0}(\nu_{31}^0)^2\pi\chi \right) \\
 K_{31}^{13} &= K_{13}^{31} = \frac{E_1^0\nu_{31}^0}{(\nu_{13}^0\nu_{31}^0 - 1)^2} \left((1 - \nu_{13}^0\nu_{31}^0) - R\sqrt{E_3^0}\pi\chi \right) \\
 K_{33}^{33} &= \frac{E_3^0}{(\nu_{13}^0\nu_{31}^0 - 1)^2} \left((1 - \nu_{13}^0\nu_{31}^0) - R\sqrt{E_3^0}\pi\chi \right) \\
 K_{11}^{33} &= G_{13}^0 \left(1 - R\frac{\pi}{\sqrt{E_1^0}}G_{13}^0\chi \right)
 \end{aligned} \tag{18}$$

179 where $\chi = \left(\frac{1}{G_{13}^0} - 2\frac{\nu_{13}^0}{E_1^0} + \frac{2}{\sqrt{E_1^0E_3^0}} \right)^{\frac{1}{2}}$, and E_1^0 , E_3^0 , G_{13}^0 , ν_{13}^0 and ν_{31}^0 are the
 180 in-plane elastic orthotropic moduli of the matrix.

181 Also in this case, the engineering moduli can be derived. The effective
 182 Young's modulus in normal direction (\mathbf{i}_3), adopted for next examples below,
 183 reads as:

$$E_3 = E_3^0 (1 - 2R H_{nn} E_3^0) \tag{19}$$

184 with H_{nn} an elastic parameter depending on the matrix and microcracks
 185 characteristics [49] (analogous to the parameter B_{nn} of the KS model).

186 3.2. Damage evolution law

187 The proposed hard interface law expressed by Eqs. (12)-(13) in the limit
 188 configuration (Fig. 2c), or by Eqs. (14)-(15) in the reference configuration
 189 (Fig. 2a), depends on the generalized microcracks density R via the effective
 190 stiffness tensors expressed by Eqs. (16) and Eqs. (18) for the KS and WG
 191 model, respectively.

192 A possible evolution law of R in the interphase \mathcal{B}^ε (of thickness ε) is herein
 193 derived following a thermodynamic approach [6, 7]. A pseudo-potential of

194 dissipation Φ given by the sum of a quadratic term and a positively 1-
 195 homogeneous functional is considered [7]. The dissipative character of the
 196 evolution of damage is given by the rate-dependent form of the potential:

$$\Phi(\dot{R}) = \frac{1}{2} \eta^\varepsilon \dot{R}^2 + I_{[0,+\infty[}(\dot{R}), \quad (20)$$

197 where η^ε is a positive viscosity parameter; $I_{\mathcal{A}}$ denotes the indicator function
 198 of the set \mathcal{A} , i.e. $I_{\mathcal{A}}(x) = 0$ if $x \in \mathcal{A}$ and $I_{\mathcal{A}}(x) = +\infty$ otherwise; \dot{R} is the
 199 increment of microcracks density compared to its initial level, indicated in
 200 what follows as R_0 . The term $I_{[0,+\infty[}(\dot{R})$ forces \dot{R} to assume non-negative
 201 values and it gives the irreversible character of the degradation process for a
 202 non-regenerative microcracked material ($R \geq R_0$).

203 The free energy associated with the constitutive equation of the micro-
 204 cracked material is chosen as follows:

$$\Psi(\mathbf{e}(\mathbf{u}^\varepsilon), R) = \frac{1}{2} \mathbb{B}^\varepsilon(R) (\mathbf{e}(\mathbf{u}^\varepsilon) : \mathbf{e}(\mathbf{u}^\varepsilon)) - \omega^\varepsilon R + I_{[R_0,+\infty[}(R) \quad (21)$$

205 where $\mathbb{B}^\varepsilon(R)$ is the effective stiffness tensor of the material (obtained via the
 206 KS or WG model); \mathbf{u} is the displacement field; $\mathbf{e}(\mathbf{u})$ is the strain tensor under
 207 the small perturbation hypothesis, ω^ε is a strictly negative parameter. Note
 208 that the irreversible character of damage, already imposed in Eq. (20), allows
 209 to neglect the term $I_{[R_0,+\infty[}(R)$ in Eq. (21).

210 By deriving Eqs. (20) and (21) with respect \dot{R} and R respectively, then
 211 by replacing them into the movement equations in \mathcal{B}^ε (for further details
 212 refer to [6, 53]), the following damage evolution law for \dot{R} in the volume \mathcal{B}^ε
 213 is obtained:

$$\eta^\varepsilon \dot{R} = \left(\omega^\varepsilon - \frac{1}{2} \mathbb{B}_{,R}^\varepsilon(R) (\mathbf{e}(\mathbf{u}^\varepsilon) : \mathbf{e}(\mathbf{u}^\varepsilon)) \right)_+ \quad (22)$$

214 where $(\cdot)_+$ denotes the positive part of the function and $\mathbb{B}_{,R}^\varepsilon(R)$ indicates
 215 the component-wise derivative of the stiffness tensor with respect to the
 216 generalized microcracks density R .

217 3.2.1. Asymptotic theory

218 In this section, the asymptotic behavior of the volumetric damage evolu-
 219 tion law (Eq. (22)) is studied. It is prescribed that η^ε and ω^ε are volumetric
 220 densities and thus they are inversely proportional to the non-dimensional
 221 interphase thickness ε : $\eta^\varepsilon = \eta \varepsilon^{-1}$ and $\omega^\varepsilon = \omega \varepsilon^{-1}$, with $\eta > 0$ and $\omega < 0$.
 222 Subsequently, for the sake of simplicity, we will further assume that ω and η
 223 do not depend on the direction orthogonal to the interface surface x_3 (respec-
 224 tively z_3 , in the rescaled configuration). In the following, also R is supposed
 225 to be independent of x_3 (respectively z_3).

226 Let focus on the term: $\frac{1}{2} \mathbb{B}_{,R}^\varepsilon(R) (\mathbf{e}(\mathbf{u}^\varepsilon) : \mathbf{e}(\mathbf{u}^\varepsilon))$ in Eq. (22). This term can
 227 be developed at 0-order as $\frac{1}{2} \mathbb{B}_{,R}^\varepsilon(R) (\hat{\mathbf{e}}^0 : \hat{\mathbf{e}}^0)$ and the constitutive equation
 228 (4b) leads to $\frac{1}{2} \mathbb{B}_{,R}^\varepsilon(R) [(\mathbb{B}^\varepsilon)^{-1}(R) \hat{\sigma}^0 : \hat{\mathbf{e}}^0]$. Note that:

$$\hat{\mathbf{e}}^0 = Sym(\hat{u}_{,1}^0 \otimes i_1 + \hat{u}_{,2}^0 \otimes i_2 + \hat{u}_{,3}^1 \otimes i_3) \quad (23)$$

229 where Sym gives the symmetric part of the enclosed tensor. This term is inte-
 230 grated along z_3 and gives $\frac{1}{2} \mathbb{B}_{,R}^\varepsilon(R) [(\mathbb{B}^\varepsilon)^{-1}(R) \hat{\sigma}^0 : \langle \hat{\mathbf{e}}^0 \rangle]$ or $\frac{1}{2} \mathbb{B}_{,R}^\varepsilon(R) (\hat{\mathbf{e}}^0 : \langle \hat{\mathbf{e}}^0 \rangle)$.
 231 Next, by integrating again along z_3 , it gives $\frac{1}{2} \mathbb{B}_{,R}^\varepsilon(R) (\langle \hat{\mathbf{e}}^0 \rangle : \langle \hat{\mathbf{e}}^0 \rangle)$, where

$$\langle \hat{\mathbf{e}}^0 \rangle = Sym(\hat{u}_{,1}^0 \otimes i_1 + \hat{u}_{,2}^0 \otimes i_2 + [\hat{u}^1] \otimes i_3) \quad (24)$$

232 Finally, by adopting the following approximation:

$$Sym(\hat{u}_{,1}^0 \otimes i_1 + \hat{u}_{,2}^0 \otimes i_2 + [\hat{u}^1] \otimes i_3) \approx Sym(\hat{u}_{,1}^\varepsilon \otimes i_1 + \hat{u}_{,2}^\varepsilon \otimes i_2 + \frac{1}{\varepsilon} [\hat{u}^\varepsilon] \otimes i_3) \quad (25)$$

233 the (internal) damage evolution equation reads:

$$\eta\dot{R} = \left\{ \omega - \frac{1}{2} K_{,R}^\varepsilon(R) \begin{pmatrix} \langle u_{,1}^\varepsilon \rangle \\ \langle \hat{u}_{,2}^\varepsilon \rangle \\ [\hat{u}^\varepsilon] \end{pmatrix} \cdot \begin{pmatrix} \langle \hat{u}_{,1}^\varepsilon \rangle \\ \langle \hat{u}_{,2}^\varepsilon \rangle \\ [\hat{u}^\varepsilon] \end{pmatrix} \right\}_+ \quad (26)$$

where

$$K^\varepsilon = \begin{pmatrix} \varepsilon K^{11} & \varepsilon K^{12} & K^{13} \\ \varepsilon K^{12} & \varepsilon K^{22} & K^{23} \\ K^{13} & K^{23} & \frac{1}{\varepsilon} K^{33} \end{pmatrix}$$

234 By introducing the matching conditions of the hard interface law (Eqs. (14)-
 235 (15)) and neglecting the second-order terms, the final form of the proposed
 236 damage evolution law for a hard interface model reads:

$$\eta\dot{R} = \left\{ \omega - \frac{1}{2} K_{,R}(R) \begin{pmatrix} \langle\langle u_{,1}^\varepsilon \rangle\rangle \\ \langle\langle u_{,2}^\varepsilon \rangle\rangle \\ [[u^\varepsilon]] + \varepsilon \langle\langle u_{,3}^\varepsilon \rangle\rangle \end{pmatrix} \cdot \begin{pmatrix} \langle\langle u_{,1}^\varepsilon \rangle\rangle \\ \langle\langle u_{,2}^\varepsilon \rangle\rangle \\ [[u^\varepsilon]] + \varepsilon \langle\langle u_{,3}^\varepsilon \rangle\rangle \end{pmatrix} \right\}_+ \quad (27)$$

237 3.3. Connection of the generalized cracks density with normalized damage 238 parameters

239 In the classical continuum damage theory at least one normalized damage
 240 variable is adopted to describe non-localized damage [6, 53, 54]. The simplest
 241 relationship to describe material properties degradation is $E = E^0(1 - D)$,
 242 where E^0 is the Young's modulus of the undamaged material and D is the
 243 damage variable going from 0 in undamaged conditions to 1 in fully damaged
 244 conditions. This damage description is generally used in commercial software
 245 for finite element analysis (FEA). Connection relationships between D and
 246 the generalized cracks density R can be obtained for both KS and WG model

247 by using Eq.(17) and Eq.(19), respectively, and they read as:

$$\begin{aligned} D &= \frac{2 R B_{nn} E^0}{1 + 2 R B_{nn} E^0} && \text{for KS model} \\ D &= 2 R H_{nn} E^0 && \text{for WG model} \end{aligned} \quad (28)$$

248 Equations (28) show that in undamaged conditions ($D = R = 0$) for both
249 damaged-material models. Instead, in fully damaged conditions ($D = 1$),
250 $R \rightarrow +\infty$ for the KS model and it is bounded by the value $R = 1/2 H_{nn} E^0$
251 for the WG model. Note that to have an upper bound for R , in the WG
252 model, is consistent with the dilute limit theory, on which the WG model is
253 based [40], meaning that the model is valid for small density values. These
254 connection relationships (28) have a twofold advantage: (i) they allow a
255 microstructural interpretation of the damage variable D , by making explicit
256 its dependency on material and microcracks properties; (ii) they are expected
257 to simplify the implementation of the proposed interface model in commercial
258 FEA-software for future validation with numerical simulation.

259 4. Numerical examples

260 Hereafter, two academic examples are used to illustrate the constitutive
261 and structural behavior of the proposed hard interface model with micro-
262 cracking damage. All the numerical computations have been carried out
263 using the commercial software *Mathematica* [55].

264 4.1. 0-D example: The constitutive behavior

265 In this section, a 0-D example is developed to illustrate the constitutive
266 behavior of the interface model. Different points are discussed: the compari-
267 son between damaged material models KS and WG; the influence of damage

268 parameters η and ω on the interface law; and finally, the influence of the
 269 loading rate and of cyclic loads on the interface behavior.

270 4.1.1. Effects of the damage evolution law

271 The mechanical properties of the damaged material (Young's modulus
 272 $E_d(E_u, R)$) in the case of KS (Eq. (17)) and WG (Eq. (19)) models, read as
 273 follows:

$$\begin{aligned} E_d^{KS}(E_u, R) &= \frac{E_u}{1 + 2\pi R} && \text{for KS model} \\ E_d^{WG}(E_u, R) &= E_u (1 - 2\pi R) && \text{for WG model} \end{aligned} \quad (29)$$

274 where $B_{nn} = H_{nn} = \frac{\pi}{E_u}$. By deriving with respect R one obtains:

$$\begin{aligned} (E_d^{KS})_{,R} &= -\frac{2\pi E_u}{(1 + 2\pi R)^2} && \text{for KS model} \\ (E_d^{WG})_{,R} &= -2\pi E_u && \text{for WG model} \end{aligned} \quad (30)$$

275 The damage evolution laws in the 0-D case, for both KS and WG models,
 276 are obtained substituting Eqs. (30) into Eq. (27):

$$\eta \dot{R} = \begin{cases} \left(\omega - \frac{1}{2} \frac{(E_d^{KS})_{,R} [u]_n^2}{\varepsilon} \right)_+ & \text{for KS model} \\ \left(\omega - \frac{1}{2} \frac{(E_d^{WG})_{,R} [u]_n^2}{\varepsilon} \right)_+ & \text{for WG model} \end{cases} \quad (31)$$

277 Equations (31) have been numerically solved with an imposed displacement
 278 jump equal to $[u]_n = [u]_{max} \frac{t}{t_f}$ with $[u]_{max} = 0.1$ mm and $t_f = 5$ s. Note that
 279 the time unit (s) is only qualitative and the proposed model does not depend
 280 on it because the interface model is developed in a quasi-static framework.
 281 Moreover, let $E_u = 70 \times 10^3$ MPa and $\varepsilon = 2$ mm. The chosen reference
 282 values for damage parameters are $\eta = 30$ MJ.s/mm² and $\omega = -2$ MJ/mm².
 283 Initial damage was imposed to vanish ($R_0 = 0$). To investigate the effects

284 of parameters η and ω on the interface model, a one-factor-a-time (OFAT)
 285 study on both η and ω has been made on ranges $\eta = (0.3, 3, 30, 300)$ and
 286 $\omega = (-0.2, -2, -20, -200)$.

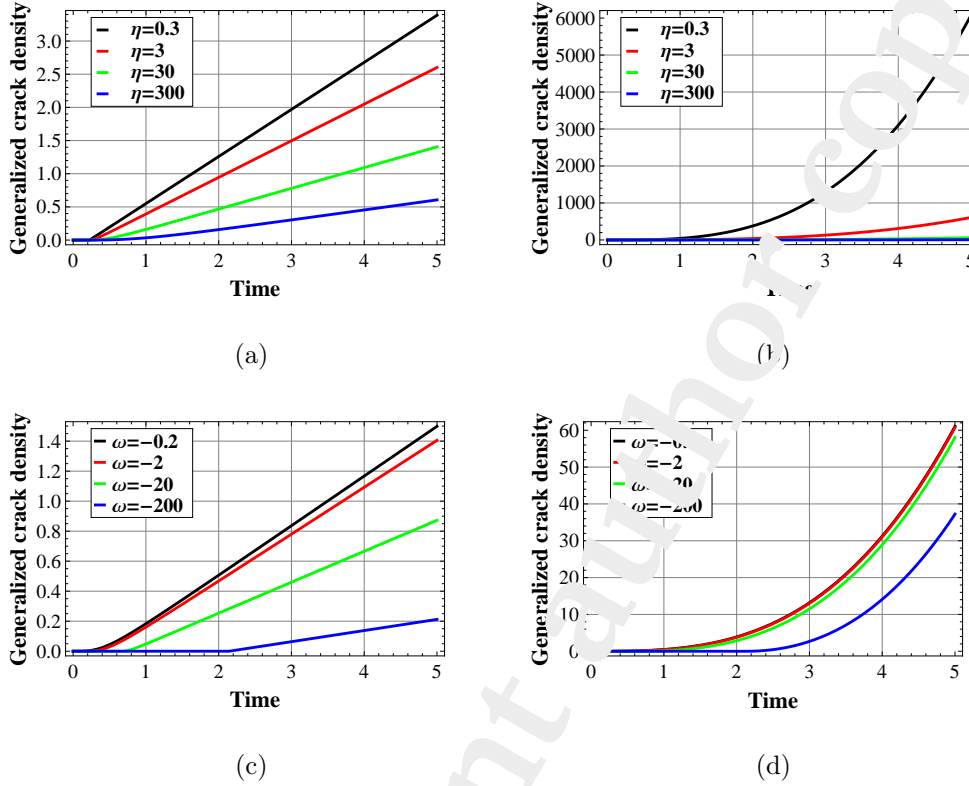


Fig. 3: Evolution of the generalized microcracks density R . Fig. 3(a):
 effect of varying η in the KS model. Fig. 3(b): effect of varying η in the
 WG model. Fig. 3(c): effect of varying ω in the KS model. Fig. 3(d): effect
 of varying ω in the WG model.

287 Figures 3a-d show the evolution of the generalized microcracks density
 288 R as a function of the time and of damage parameters η and ω , for both
 289 KS and WG models. At the beginning, both models present an horizontal

290 plateau at zero (because of the imposed initial damage $R_0 = 0$); then, after
 291 damage initiation, a linear increasing behavior is found for the KS model and
 292 a cubic increasing behavior for the WG model. An inverse proportionality
 293 between R and η is found in both models (see Fig. 3(a) and Fig. 3(b)), this
 294 highlights that η has the physical meaning of a damage viscosity influencing
 295 the velocity (slope of (R, t) curves) of the damage evolution. This result is
 296 also emphasized in Fig. 4, where the degradation of the Young's modulus
 297 of both damaged materials KS and WG is shown. The slope of $(E_d/E_u, t)$
 298 curves, for both KS and WG models, increases as η decreases, meaning that
 299 material get damaged "faster" for smaller values of η .

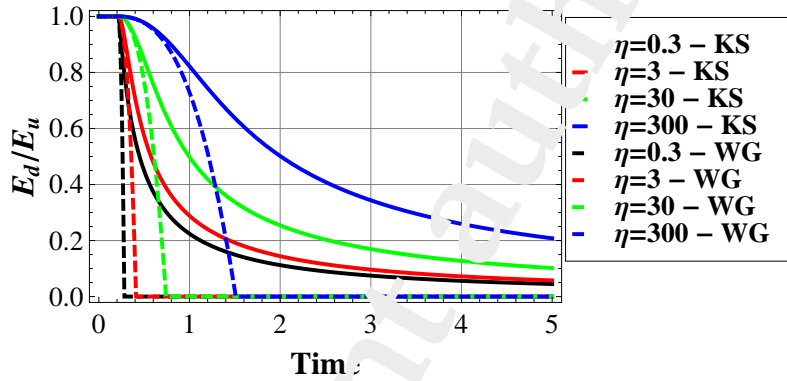


Fig. 4: Evolution in time of the Young's modulus of the damaged materials: parametric study on η . Kachanov, Sevostianov (KS, solid lines) and Welemane-Goidescu (WG, dashed lines) damaged material models are represented.

300 The parameter η has the physical meaning of a threshold energy beyond
 301 which damage initiates, in analogy with Dupré's energy for adhesion [53]. In
 302 fact, the damage-initiation time, *i.e.*, when R begins to increase, is more

303 influenced by ω than by η for both damaged materials, as highlighted in
 304 Figs. 3(c), 3(d) and 5.

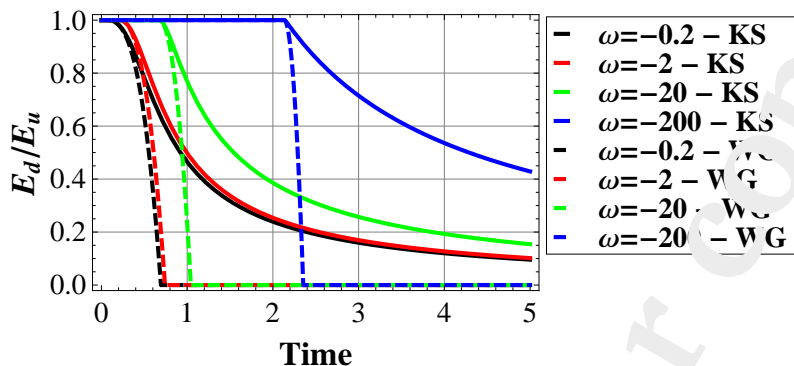


Fig. 5: Evolution in time of the Young's modulus of the damaged materials: parametric study on ω . Kachanov-Sevostianov model (KS, solid lines) and Welemane-Goidescu model (WG, dashed lines).

304

305 Moreover, Figs. 4 and 5 show that the complete damage (*i.e.*, when E_d
 306 tends to zero) occurs earlier for the WG model than for the KS model inde-
 307 pendently of ω and η . Note that in the case of KS model, E_d tends to zero
 308 asymptotically (data not shown). This different behavior of the two models is
 309 consistent with the two different hypotheses on which the models are based.
 310 Particularly, WG model is based on the dilute limit hypothesis, meaning that
 311 it is valid for small density values (less than 20% according to [39]). This is
 312 also in agreement with the fact that the generalized cracks density R has an
 313 upper bound in the case of WG model (see Section 3.3). The KS model is
 314 based on the non-interacting microcracks approximation and it is valid for
 315 greater microcracks densities (until 80% according to [36, 37]). For further

316 details regarding the difference between these microstructural hypotheses the
 317 reader can refer to [37].

318 The interface model in 0-D can be expressed as:

$$\sigma_n = \frac{E_d}{\varepsilon} [u]_n \quad (32)$$

319 Equation (32) has been solved for both KS and WG models, replacing E_d by
 320 E_d^{KS} and E_d^{WG} , respectively (see Eqs. (29)), in which R has been obtained
 by Eqs. (31).

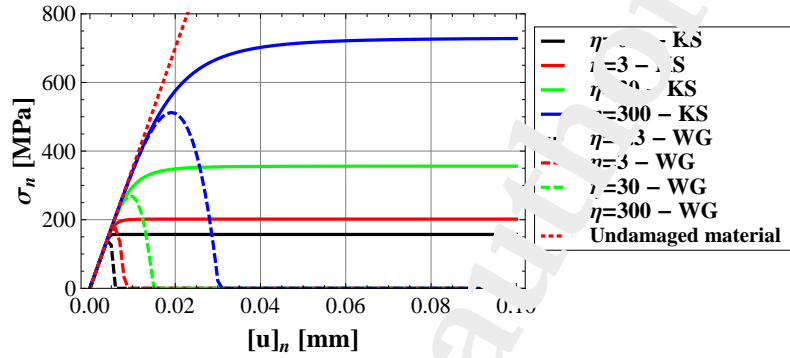


Fig. 6: Interface law: parametric study on η . Kachanov-Sevostianov (KS, solid lines) and Welemane-Goidescu (WG, dashed lines) damaged material models are represented. The linear-elastic behavior of the undamaged material is represented with a red dotted line.

321

322 Figures 6 and 7 show the interface model for both damaged materials as a
 323 function of η and ω . Numerical curves are obtained by solving the damaged
 324 interface model (Eq. (32), (29), and (31)) in displacement-controlled mode.
 325 Both figures suggest a brittle damage behavior in the case of WG model and
 326 a ductile damage behavior for the KS model. Figure 6 highlights that the

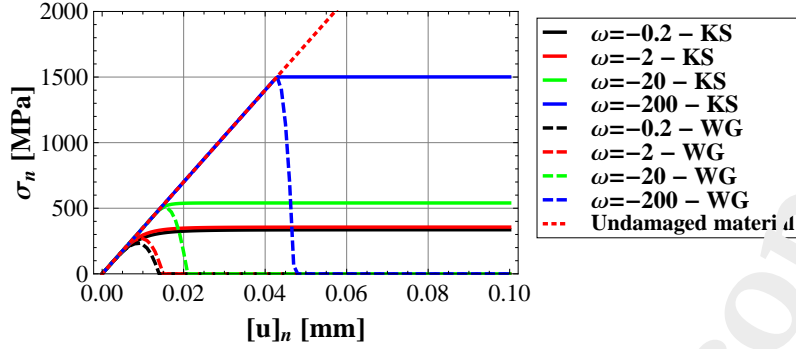


Fig. 7: Interface law: parametric study on ω . Kachanov-Sevostianov (KS, solid lines) and Welemane-Goidescu (WG, dashed lines) damage material models are represented. The linear-elastic behavior of the undamaged material is represented with a red dotted line.

327 elastic limit increases with η and this result confirms the role of the damage
 328 viscosity η as the velocity of the damage evolution. Figure 6 shows also that η
 329 influences the nonlinear transition between the linear elastic domain and the
 330 damaged domain (this is more evident in KS model than in WG model); thus
 331 for a small damage viscosity η this transition tends to vanish (*i.e.*, suggesting
 332 that the material gets damaged immediately after the initiation). Figure 7
 333 emphasizes the role of parameter ω as a damage initiation threshold: thus
 334 the higher is ω , the later damage initiates (see Fig. 5) and the higher the
 335 elastic limit.

336 4.1.2. Effects of the loading rate

337 The influence of the loading rate and of the loading shape on the interface
 338 model has been investigated. In particular, two displacement jumps have

339 been separately imposed to solve Eqs. (32), (29), and (31): a ramp function
 340 $[u]_n = v t$ and a quadratic function $[u]_n = 1/2 v^2 t^2 + 1/2 v t$. Four values of the
 341 loading rate $v = [u]_{max} / t_f$ have been simulated (0.1, 0.2, 2, 20) mm/s with a
 342 fixed $[u]_{max} = 1$ mm and by varying the duration t_f between (0.05, 0.5, 5, 10)
 343 s. The damage parameters have been taken equal to their reference values
 344 $\eta = 30$ MJ.s/mm² and $\omega = -2$ MJ/mm². The other parameters $\sigma_u =$
 70×10^3 MPa, $\varepsilon = 2$ mm and $R_0 = 0$, are taken as in the previous study.

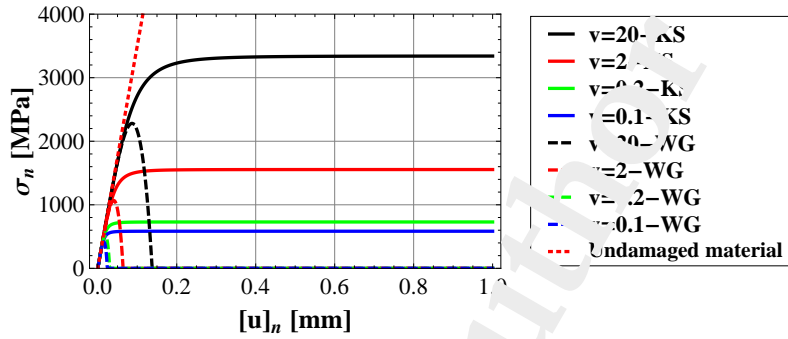


Fig. 8: Interface law for a ramp displacement jump: parametric study on the loading rate v . Kachanov-Sevostianov (KS, solid lines) and Welemane-Goidescu (WG, dashed lines) damaged material models are represented. The linear-elastic behavior of the undamaged material is represented with a red dotted line.

345

346 Figure 8 shows the interface law in the case of the ramp displacement
 347 jump. In analogy with the previous section, a ductile damage behavior of the
 348 interface is obtained in the case of KS model and a brittle damage behavior
 349 for WG model.

350 Figure 9 shows the interface law in the case of the quadratic displacement
 351 jump. The imposed quadratic displacement jump produces an hardening-like

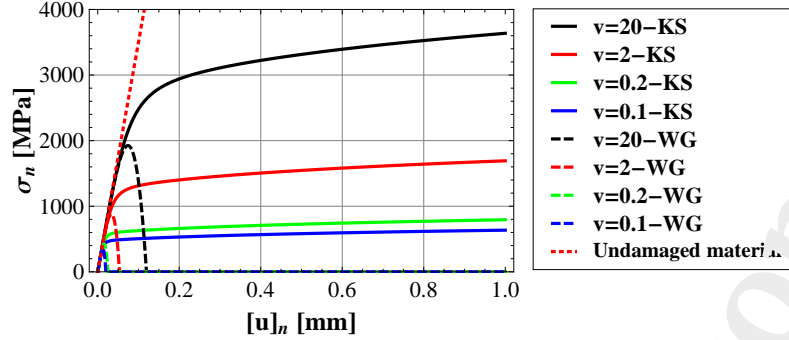


Fig. 9: Interface law for a quadratic displacement-jump: parametric study on the loading rate v . Kachanov-Sevostianov (KS, solid lines) and Welemane-Goidescu (WG, dashed lines) damaged material models are represented. The linear-elastic behavior of the undamaged material is represented with a red dotted line.

352 effect in the damaged part of the interface constitutive behavior (*i.e.*, beyond
 353 the elastic limit) and the slope increases with the loading rate v .

354 Both Figs. 8-9 highlight that for high rates ($v = 2, 20$ mm/s) the elastic
 355 limit (tensile) is higher than in the quasi-static configurations ($v = 0.1, 0.2$
 356 mm/s) for both KS and WG models. Recently, authors provide a validation
 357 of the proposed hard interface model in [31], by comparing simulated response
 358 curves with data from tensile experimental tests available in the literature
 359 [56] in both quasi-static and high-rate loading conditions. They found that
 360 the loading-rate dependence of the hard interface model makes it suitable to
 361 describe the experimental behavior observed in [56].

362 4.1.3. Effects of cyclic loading

363 The influence of cyclic loading on the hard interface model has also been
 364 investigated. A strictly positive sinusoidal displacement jump has been im-

365 posed: $[u]_n = [u]_{max} |\sin(f t/t_f)|$, with $[u]_{max} = 1$ mm, $f = \pi/2$, $t_f = 5$ s
 366 and 5 cycles have been considered. Both KS and WG damage models have
 367 been considered and the damage parameters have been taken equal to their
 368 reference values $\eta = 30$ MJ.s/mm² and $\omega = -2$ MJ/mm². $E_u = 10 \times 10^3$
 MPa, $\varepsilon = 2$ mm and $R_0 = 0$, as in the previous study.

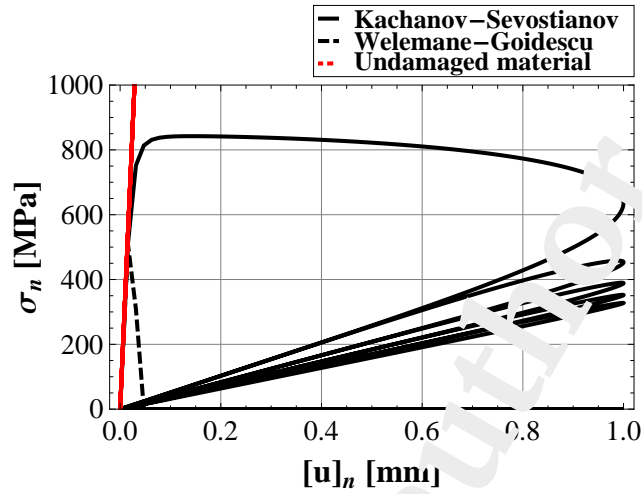


Fig. 10: Interface law for a cyclic load for KS and WG model. The linear-elastic behavior of the undamaged material is represented with a red dotted line.

369

370 As shown in Fig. 10, the two damage models give very different results
 371 under the same loading and parameter conditions. KS model, together with
 372 the proposed damage evolution law, is able to reproduce an elastic-damaged
 373 material behavior with hysteresis, as illustrated in Fig. 10. Generally, the en-
 374 ergy dissipated via micro-cracking damage is higher at the initiation and first
 375 accumulation of microcracks. This is consistent with the resulting hysteresis
 376 loop of the first cycle that is larger than the others; after the first cycle, the

377 hysteresis decreases with the number of cycles until the damage evolution
 378 is completed. Moreover, the damage evolution produces a decreasing of the
 379 interface stiffness (see Fig. 10). The stiffness of the undamaged material is
 380 equal to 35000 N/mm^3 and after the first cycle it reduces to 515 N/mm^3 .
 381 After the first reloading (2nd cycle), the stiffness slightly decreases until the
 382 damage evolution is completed, and at the end of the fifth cycle the stiffness
 383 is equal to 318 N/mm^3 . This result is physically plausible.

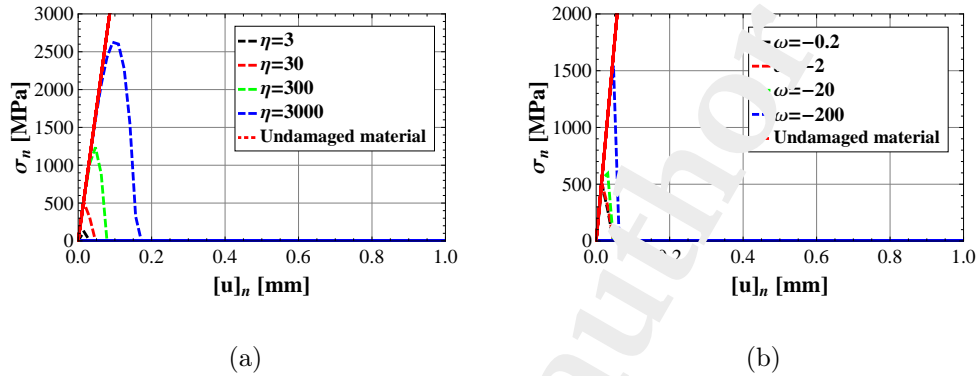


Fig. 11: Interface law for a cyclic load for WG model. Fig. 11(a): study on η .
 Fig. 11(b): study on ω .

384 On the contrary, WG damage model is not able to reproduce a damage
 385 behavior under cyclic loads. Figure 10 shows an abrupt reduction in stiffness
 386 to zero already during the first loading curve, meaning that the damaged
 387 material behavior is brittle, in agreement with the previous results. Note
 388 that this behavior does not depend on the chosen values of the damaged
 389 parameters η and ω as illustrated in Fig. 11.

390 Finally, Fig. 12 shows the evolution in time of the normal stress σ_n in the
 391 case of KS model, highlighting the decrease of the maximum normal stress

392 with the number of cycles (note a decrease of the 60% at the last cycle).

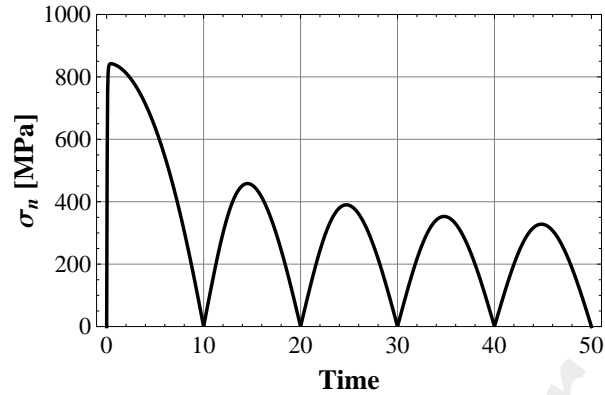


Fig. 12: Interface law for a cyclic load: normal stress as a function of the time for the Kachanov-Sevostianov damage model.

393 4.2. 1-D example: The structural behavior

394 In this section, a simple 1-D example is developed to illustrate the struc-
395 tural behavior of the proposed hard interface model. A composite bar under
396 traction was considered. The bar, of section A , comprised two parts of length
397 ℓ , made of an undamaged material with Young's modulus E_u , and an embed-
398 ded part of length ε , made of a damageable material (glue-like interphase)
399 with Young's modulus $E_d(E_u, R)$. The damageable material in the inter-
400 phase is supposed to have at the beginning the same Young's modulus of the
401 adherents, then it degrades as the microcracks density R evolves. The bar
402 was fixed at one end and a quasi-static traction force was $F(t)$ applied on
403 the other end, as illustrated in Fig. 13.

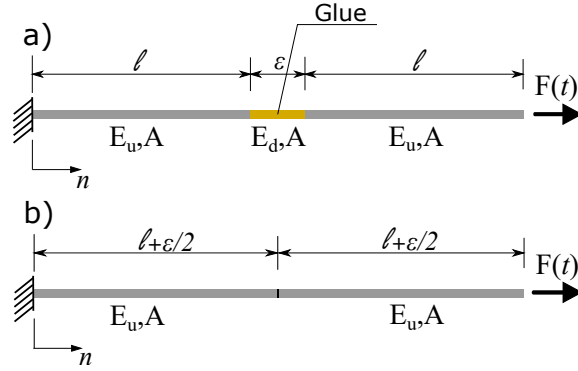


Fig. 13: 1-D example: bar under traction, a) glue interphase, b) interface model

404 The displacement field can be easily derived analytically as:

$$u(n) = \begin{cases} \frac{F}{E_u A} n & 0 \leq n \leq l \\ \frac{F}{E_d A} n + \frac{F l}{A} \left(\frac{1}{E_u} - \frac{1}{E_d} \right) & l \leq n \leq l + \varepsilon \\ \frac{F}{E_u A} n - \frac{F \varepsilon}{A} \left(\frac{1}{E_u} - \frac{1}{E_d} \right) & l + \varepsilon \leq n \leq 2l + \varepsilon \end{cases} \quad (33)$$

405 Thus, the displacement jump along n is obtained as $[u]_n = u(l + \varepsilon) - u(l)$:

$$[u]_n = \frac{F \varepsilon}{E_u A} \quad (34)$$

406 Note that, being $\frac{F}{A} = \sigma_n$, the standard spring-like interface law in 1-D ap-
407 proximation can be derived (in analogy with Eq. (32)).

408 The Young's modulus of the damaged material $E_d(E_u, R)$ was specialized
409 to the case of KS and WG model following Eqs. (29) as in the previous
410 example. The expression of the evolution of damage Eqs. (31) taking into
411 account the displacement jump Eq. (34) is derived in this 1-D case as:

$$\dot{R} = \begin{cases} \frac{1}{\eta} \left(\omega + \pi \frac{\sigma_n^2}{E_u} \varepsilon \right)_+ & \text{for KS model} \\ \frac{1}{\eta} \left(\omega + \pi \frac{\sigma_n^2}{E_u} \varepsilon \frac{1}{(1 - 2\pi R)^2} \right)_+ & \text{for WG model} \end{cases} \quad (35)$$

412 where $\sigma_n = \bar{\sigma} \bar{t}$ with $\bar{t} = \frac{t}{t_f} \in [0, 1]$, $t_f = 5$ s and $\bar{\sigma} = 400$ MPa. Moreover,
 413 reference values are taken as previously: $E_u = 70 \times 10^3$ MPa, $\varepsilon = 2$ mm,
 414 $\eta = 30$ MJ.s/mm² and $\omega = -2$ MJ/mm².

415 The structural response of the proposed hard interface model, in terms
 416 of tensile stress as a function of the macroscopic displacement jump is il-
 417 lustrated in Fig. 14, where we find again a brittle behavior for weak material
 and a ductile behavior for KS material.

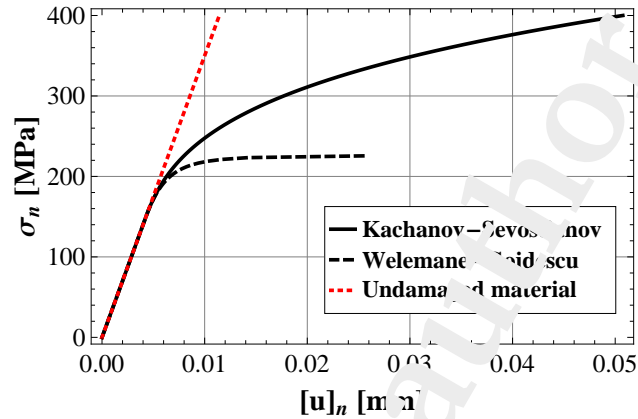


Fig. 14: Interface law in the 1-D case (Kachanov-Sevostianov model (KS, solid line), Welemane-Goidescu model (V.G., dashed line), undamaged material (red dotted line)).

418

419 5. Conclusions

420 This work proposes an original model of hard imperfect interface account-
 421 ing for micro-cracking and damage evolution. Preliminary numerical results
 422 based on simple academic examples, in terms of both constitutive and struc-

423 tural behavior, are promising. They suggest that the model could repre-
424 sent a suitable strategy for a macroscopic description of hard adhesives with
425 micro-cracking damage, regardless of whether they have a ductile or brittle
426 behavior. In fact, the analytical interface model could be included in a finite
427 element context via user-defined interface finite elements. Moreover, connec-
428 tion relationships between the generalized cracks density and the standard
429 normalized damage variable, derived at Section 3.3, are expected to simplify
430 the implementation in commercial FEA-software for future validation with
431 numerical simulation.

432 The main perspective to enhance the proposed model is to establish a
433 combined experimental/modelling identification protocol for the damage pa-
434 rameters of the evolution law, the damage viscosity η and the damage thresh-
435 old ω . A design of experience will be set up in order to catch the interactions
436 between damage parameters η and ω that we could only glimpse through the
437 OFAT approach. To this aim, authors have specialized the proposed hard
438 interface model to the case of tubular-butt joints under combined tensile-
439 torsion loads [31]. This is a standard experimental design used to charac-
440 terize structural adhesives and it allows future validations of the proposed
441 interface model with experimental tests.

442 **A. Matched asymptotic expansions method**

443 *A.1. Rescaling phase*

444 The rescaling phase of the asymptotic process represents a mathematical
445 construct [46], in a physically-based configuration, and it is used in order to
446 eliminate the dependency of the integration domains on the small parameter

447 ε . This construct can also be seen as a change of spatial variables in the
 448 interphase domain [45, 46] $\hat{\mathbf{p}} := (x_1, x_2, x_3) \rightarrow (z_1, z_2, z_3)$:

$$z_1 = x_1, \quad z_2 = x_2, \quad z_3 = \frac{x_3}{\varepsilon} \quad (\text{A.1})$$

449 resulting

$$\frac{\partial}{\partial z_1} = \frac{\partial}{\partial x_1}, \quad \frac{\partial}{\partial z_2} = \frac{\partial}{\partial x_2}, \quad \frac{\partial}{\partial z_3} = \varepsilon \frac{\partial}{\partial x_3} \quad (\text{A.2})$$

450 as well as in the adherents $\bar{\mathbf{p}} := (x_1, x_2, x_3) \rightarrow (z_1, z_2, z_3)$:

$$z_1 = x_1, \quad z_2 = x_2, \quad z_3 = x_3 \pm \frac{1}{2}(1 - \varepsilon) \quad (\text{A.3})$$

451 where the plus (minus) sign applies whenever $x \in \Omega_+$ ($x \in \Omega_-$), with

$$\frac{\partial}{\partial z_1} = \frac{\partial}{\partial x_1}, \quad \frac{\partial}{\partial z_2} = \frac{\partial}{\partial x_2}, \quad \frac{\partial}{\partial z_3} = \frac{\partial}{\partial x_3} \quad (\text{A.4})$$

452 After the change of variables (A.1) and (A.3), the interphase occupies the
 453 domain $\mathcal{B} = \{(z_1, z_2, z_3) \in \mathbb{R}^3 : (z_1, z_2) \in \mathcal{S} \mid |z_3| < \frac{1}{2}\}$ and the adherents
 454 occupy the domains $\Omega_{\pm} = \Omega^{\varepsilon}_{\pm} \pm \frac{1}{2}(1 - \varepsilon)\mathbf{1}_3$, as shown in Fig. 2b. The sets
 455 $\mathcal{S}_{\pm} = \{(z_1, z_2, z_3) \in \mathbb{R}^3 : (z_1, z_2) \in \mathcal{S} \mid z_3 = \pm \frac{1}{2}\}$ are taken to denote the
 456 interfaces between \mathcal{B} and Ω_{\pm} and $\Omega = \Omega_+ \cup \Omega_- \cup \mathcal{B} \cup \mathcal{S}_+ \cup \mathcal{S}_-$ is the rescaled
 457 configuration of the composite body. Γ_u and Γ_g indicate the images of Γ_u^{ε}
 458 and Γ_g^{ε} after the change of variables, and $\bar{\mathbf{f}}^{\pm} := \mathbf{f}^{\pm} \circ \bar{\mathbf{p}}^{-1}$ and $\bar{\mathbf{g}}^{\pm} := \mathbf{g}^{\pm} \circ \bar{\mathbf{p}}^{-1}$
 459 the rescaled external forces.

460 A.2. Kinematic equations

Following the approach proposed in [23, 25], let us focus on the kinematics of the elastic problem. After taking $\hat{\mathbf{u}}^{\varepsilon} = \mathbf{u}^{\varepsilon} \circ \hat{\mathbf{p}}^{-1}$ and $\bar{\mathbf{u}}^{\varepsilon} = \mathbf{u}^{\varepsilon} \circ \bar{\mathbf{p}}^{-1}$ to

denote the displacement fields from the rescaled adhesive and adherents, respectively, the asymptotic expansions of the displacement fields with respect to ε are:

$$\mathbf{u}^\varepsilon(x_1, x_2, x_3) = \mathbf{u}^0 + \varepsilon \mathbf{u}^1 + \varepsilon^2 \mathbf{u}^2 + o(\varepsilon^2) \quad (\text{A.5a})$$

$$\hat{\mathbf{u}}^\varepsilon(z_1, z_2, z_3) = \hat{\mathbf{u}}^0 + \varepsilon \hat{\mathbf{u}}^1 + \varepsilon^2 \hat{\mathbf{u}}^2 + o(\varepsilon^2) \quad (\text{A.5b})$$

$$\bar{\mathbf{u}}^\varepsilon(z_1, z_2, z_3) = \bar{\mathbf{u}}^0 + \varepsilon \bar{\mathbf{u}}^1 + \varepsilon^2 \bar{\mathbf{u}}^2 + o(\varepsilon^2) \quad (\text{A.5c})$$

461 *Interphase.* The gradient of the displacement field $\hat{\mathbf{u}}^\varepsilon$ reads:

$$\nabla(\hat{\mathbf{u}}^\varepsilon) = \varepsilon^{-1} \begin{bmatrix} 0 & \hat{u}_{\alpha,3}^0 \\ 0 & \hat{u}_{3,3}^0 \end{bmatrix} + \begin{bmatrix} \hat{u}_{\alpha,\beta}^0 & \hat{u}_{\alpha,3}^1 \\ \hat{u}_{3,\beta}^0 & \hat{u}_{3,3}^1 \end{bmatrix} + \varepsilon \begin{bmatrix} \hat{u}_{\alpha,\beta}^1 & \hat{u}_{\alpha,3}^2 \\ \hat{u}_{3,\beta}^1 & \hat{u}_{3,3}^2 \end{bmatrix} + O(\varepsilon^2) \quad (\text{A.6})$$

462 where $\alpha, \beta = 1, 2$, so that the strain tensor is:

$$\mathbf{e}(\hat{\mathbf{u}}^\varepsilon) = \frac{1}{2} [\nabla(\hat{\mathbf{u}}^\varepsilon) + \nabla(\hat{\mathbf{u}}^\varepsilon)^T] = \varepsilon^{-1} \hat{\mathbf{e}}^{-1} + \hat{\mathbf{e}}^0 + \varepsilon \hat{\mathbf{e}}^1 + O(\varepsilon^2) \quad (\text{A.7})$$

463 with:

$$\hat{\mathbf{e}}^{-1} = \begin{bmatrix} 0 & \frac{1}{2} \hat{u}_{c,3}^0 \\ \frac{1}{2} \hat{u}_{\alpha,3}^0 & \hat{u}_{\alpha,3}^0 \end{bmatrix} = \text{Sym}(\hat{\mathbf{u}}_{,3}^0 \otimes \mathbf{i}_3) \quad (\text{A.8})$$

$$\hat{\mathbf{e}}^k = \begin{bmatrix} \text{Sym}(\hat{u}_{\alpha,\beta}^k) & \frac{1}{2}(\hat{u}_{3,\alpha}^k + \hat{u}_{\alpha,3}^{k+1}) \\ \frac{1}{2}(\hat{u}_{3,\alpha}^k + \hat{u}_{\alpha,3}^{k+1}) & \hat{u}_{\alpha,3}^{k+1} \end{bmatrix} = \text{Sym}(\hat{\mathbf{u}}_{,1}^k \otimes \mathbf{i}_1 + \hat{\mathbf{u}}_{,2}^k \otimes \mathbf{i}_2 + \hat{\mathbf{u}}_{,3}^{k+1} \otimes \mathbf{i}_3) \quad (\text{A.9})$$

464 where $\text{Sym}(\cdot)$ gives the symmetric part of the enclosed tensor and $k = 0, 1$,
 465 and \otimes is the dyadic product between vectors such as: $(\mathbf{a} \otimes \mathbf{b})_{ij} = a_i b_j$.
 466 Moreover, the following notation for derivatives is adopted: $f_{,j}$ denoting the
 467 partial derivative of f with respect to z_j .

468 *Adherents.* The gradient of the displacement field $\bar{\mathbf{u}}^\varepsilon$ reads:

$$\nabla(\bar{\mathbf{u}}^\varepsilon) = \begin{bmatrix} \bar{u}_{\alpha,\beta}^0 & \bar{u}_{\alpha,3}^0 \\ \bar{u}_{3,\beta}^0 & \bar{u}_{3,3}^0 \end{bmatrix} + \varepsilon \begin{bmatrix} \bar{u}_{\alpha,\beta}^1 & \bar{u}_{\alpha,3}^1 \\ \bar{u}_{3,\beta}^1 & \bar{u}_{3,3}^1 \end{bmatrix} + O(\varepsilon^2) \quad (\text{A.10})$$

469 so that the strain tensor is:

$$\mathbf{e}(\bar{\mathbf{u}}^\varepsilon) = \frac{1}{2} [\nabla(\bar{\mathbf{u}}^\varepsilon) + \nabla(\bar{\mathbf{u}}^\varepsilon)^T] = \varepsilon^{-1} \bar{\mathbf{e}}^{-1} + \bar{\mathbf{e}}^0 + \varepsilon \bar{\mathbf{e}}^1 + O(\varepsilon^2) \quad (\text{A.11})$$

470 with:

$$\bar{\mathbf{e}}^{-1} = \mathbf{0} \quad (\text{A.12})$$

471

$$\bar{\mathbf{e}}^k = \begin{bmatrix} \text{Sym}(\bar{u}_{\alpha,\beta}^k) & \frac{1}{2}(\bar{u}_{3,\alpha}^k + \bar{u}_{\alpha,3}^k) \\ \frac{1}{2}(\bar{u}_{3,\alpha}^k + \bar{u}_{\alpha,3}^k) & \bar{u}_{3,3}^k \end{bmatrix} = \text{Sym}(\bar{\mathbf{u}}_{\alpha,1}^k \otimes \mathbf{i}_1 + \bar{\mathbf{u}}_{\alpha,2}^k \otimes \mathbf{i}_2 + \bar{\mathbf{u}}_{\alpha,3}^k \otimes \mathbf{i}_3) \quad (\text{A.13})$$

472 and $k = 0, 1$.

473 A.3. Equilibrium equations

The stress fields in the rescaled adhesive and adherents, $\hat{\boldsymbol{\sigma}}^\varepsilon = \boldsymbol{\sigma} \circ \hat{\mathbf{p}}^{-1}$ and $\bar{\boldsymbol{\sigma}}^\varepsilon = \boldsymbol{\sigma} \circ \bar{\mathbf{p}}^{-1}$ respectively, can be represented as asymptotic expansions [23, 25]:

$$\boldsymbol{\sigma} = \boldsymbol{\sigma}^0 + \varepsilon \boldsymbol{\sigma}^1 + O(\varepsilon^2) \quad (\text{A.14a})$$

$$\hat{\boldsymbol{\sigma}} = \hat{\boldsymbol{\sigma}}^0 + \varepsilon \hat{\boldsymbol{\sigma}}^1 + O(\varepsilon^2) \quad (\text{A.14b})$$

$$\bar{\boldsymbol{\sigma}} = \bar{\boldsymbol{\sigma}}^0 + \varepsilon \bar{\boldsymbol{\sigma}}^1 + O(\varepsilon^2) \quad (\text{A.14c})$$

474 *Interphase.* As body forces are neglected, the equilibrium equation is:

$$\text{div} \hat{\boldsymbol{\sigma}}^\varepsilon = \mathbf{0} \quad (\text{A.15})$$

475 Substituting Eq. (A.14b) in Eq. (A.15) and using Eq. (A.2), it becomes:

$$\begin{aligned} 0 &= \hat{\sigma}_{i\alpha,\alpha}^\varepsilon + \varepsilon^{-1} \hat{\sigma}_{i3,3}^\varepsilon \\ &= \varepsilon^{-1} \hat{\sigma}_{i3,3}^0 + \hat{\sigma}_{i\alpha,\alpha}^0 + \hat{\sigma}_{i3,3}^1 + \varepsilon \hat{\sigma}_{i\alpha,\alpha}^1 + O(\varepsilon) \end{aligned} \quad (\text{A.16})$$

476 where $\alpha = 1, 2$. Eq. (A.16) has to be satisfied for any value of ε , leading to:

$$\hat{\sigma}_{i3,3}^0 = 0 \quad (\text{A.17})$$

$$\hat{\sigma}_{i1,1}^0 + \hat{\sigma}_{i2,2}^0 + \hat{\sigma}_{i3,3}^1 = 0 \quad (\text{A.18})$$

477 where $i = 1, 2, 3$.

478 Eq. (A.17) shows that $\hat{\sigma}_{i3}^0$ is not dependent on i in the adhesive, and
479 thus it can be written:

$$[\hat{\sigma}_{i3}^0] = 0 \quad (\text{A.19})$$

480 where $[\cdot]$ denotes the jump between $z_3 = \frac{1}{5}$ and $z_3 = -\frac{1}{2}$. In view of
481 Eq. (A.19), Eq. (A.18), for $i = 3$, can be rewritten in the integrated form

$$[\hat{\sigma}_{33}^1] = -\hat{\sigma}_{13,1}^0 - \hat{\sigma}_{23,2}^0 \quad (\text{A.20})$$

482 *Adherents.* The equilibrium equation in the adherents is:

$$\text{div} \bar{\boldsymbol{\sigma}}^\varepsilon + \bar{\mathbf{f}} = \mathbf{0} \quad (\text{A.21})$$

483 Substituting Eq. (A.14c) in Eq. (A.21) that has to be satisfied for any value
484 of ε , leads to:

$$\text{div} \bar{\boldsymbol{\sigma}}^0 + \bar{\mathbf{f}} = \mathbf{0} \quad (\text{A.22})$$

$$\text{div} \bar{\boldsymbol{\sigma}}^1 = \mathbf{0} \quad (\text{A.23})$$

485 *A.4. Matching phase*

486 The imposed continuity conditions at $\mathcal{S}_{\pm}^{\varepsilon}$ for the fields \mathbf{u}^{ε} and $\boldsymbol{\sigma}^{\varepsilon}$ lead to
 487 matching relationships between external and internal expansions [23, 25]. In
 488 terms of displacements the following relationship have to be satisfied:

$$\mathbf{u}^{\varepsilon}(\mathbf{x}_{\alpha}, \pm \frac{\varepsilon}{2}) = \hat{\mathbf{u}}^{\varepsilon}(\mathbf{z}_{\alpha}, \pm \frac{1}{2}) = \bar{\mathbf{u}}^{\varepsilon}(\mathbf{z}_{\alpha}, \pm \frac{1}{2}) \quad (\text{A.24})$$

489 where $\mathbf{x}_{\alpha} := (x_1, x_2)$, $\mathbf{z}_{\alpha} := (z_1, z_2) \in \mathcal{S}$. Expanding the displacement in the
 490 adherents \mathbf{u}^{ε} , in Taylor series along the x_3 -direction and taking into account
 491 Eq. (A.5a), it results:

$$\begin{aligned} \mathbf{u}^{\varepsilon}(\mathbf{x}_{\alpha}, \pm \frac{\varepsilon}{2}) &= \mathbf{u}^{\varepsilon}(\mathbf{x}_{\alpha}, 0^{\pm}) \pm \frac{\varepsilon}{2} \mathbf{u}_{,3}^{\varepsilon}(\mathbf{x}_{\alpha}, 0^{\pm}) + \dots \\ &= \mathbf{u}^0(\mathbf{x}_{\alpha}, 0^{\pm}) + \varepsilon \mathbf{u}^1(\mathbf{x}_{\alpha}, 0^{\pm}) \pm \frac{\varepsilon}{2} \mathbf{u}_{,3}^0(\mathbf{x}_{\alpha}, 0^{\pm}) + \dots \end{aligned} \quad (\text{A.25})$$

492 Substituting Eqs. (A.5b) and (A.5c) together with Eq. (A.25) in Eq. (A.24),
 493 it holds true:

$$\begin{aligned} &\mathbf{u}^0(\mathbf{x}_{\alpha}, 0^{\pm}) + \\ &+ \varepsilon \mathbf{u}^1(\mathbf{x}_{\alpha}, 0^{\pm}) \pm \frac{\varepsilon}{2} \mathbf{u}_{,3}^0(\mathbf{x}_{\alpha}, 0^{\pm}) + \dots = \hat{\mathbf{u}}^0(\mathbf{z}_{\alpha}, \pm \frac{1}{2}) + \varepsilon \hat{\mathbf{u}}^1(\mathbf{z}_{\alpha}, \pm \frac{1}{2}) + \dots \\ &= \bar{\mathbf{u}}^0(\mathbf{z}_{\alpha}, \pm \frac{1}{2}) + \varepsilon \bar{\mathbf{u}}^1(\mathbf{z}_{\alpha}, \pm \frac{1}{2}) + \dots \end{aligned} \quad (\text{A.26})$$

494 By identifying the terms in the same powers of ε , Eq. (A.26) gives:

$$\mathbf{u}^0(\mathbf{x}_{\alpha}, 0^{\pm}) = \hat{\mathbf{u}}^0(\mathbf{z}_{\alpha}, \pm \frac{1}{2}) = \bar{\mathbf{u}}^0(\mathbf{z}_{\alpha}, \pm \frac{1}{2}) \quad (\text{A.27})$$

$$\mathbf{u}^1(\mathbf{x}_{\alpha}, 0^{\pm}) \pm \frac{\varepsilon}{2} \mathbf{u}_{,3}^0(\mathbf{x}_{\alpha}, 0^{\pm}) = \hat{\mathbf{u}}^1(\mathbf{z}_{\alpha}, \pm \frac{1}{2}) = \bar{\mathbf{u}}^1(\mathbf{z}_{\alpha}, \pm \frac{1}{2}) \quad (\text{A.28})$$

495 By identification processes, analogous results are obtained in terms of stresses
 496 [23, 25]:

$$\sigma_{i3}^0(\mathbf{x}_{\alpha}, 0^{\pm}) = \hat{\sigma}_{i3}^0(\mathbf{z}_{\alpha}, \pm \frac{1}{2}) = \bar{\sigma}_{i3}^0(\mathbf{z}_{\alpha}, \pm \frac{1}{2}) \quad (\text{A.29})$$

497

$$\sigma_{i3}^1(\mathbf{x}_\alpha, 0^\pm) \pm \frac{1}{2}\sigma_{i3,3}^0(\mathbf{x}_\alpha, 0^\pm) = \hat{\sigma}_{i3}^1(\mathbf{z}_\alpha, \pm\frac{1}{2}) = \bar{\sigma}_{i3}^1(\mathbf{z}_\alpha, \pm\frac{1}{2}) \quad (\text{A.30})$$

498 for $i = 1, 2, 3$.499 *A.5. Constitutive equations*

The constitutive laws in linear elasticity for the adherents and the interphase are considered:

$$\bar{\boldsymbol{\sigma}}^\varepsilon = \mathbb{A}_\pm(\mathbf{e}(\bar{\mathbf{u}}^\varepsilon)) \quad (\text{A.31a})$$

$$\hat{\boldsymbol{\sigma}}^\varepsilon = \mathbb{B}^\varepsilon(\mathbf{e}(\hat{\mathbf{u}}^\varepsilon)) \quad (\text{A.31b})$$

500 where $\mathbb{A}_\pm, \mathbb{B}^\varepsilon$ are the elasticity tensor of adherents and of interphase, respec-
501 tively.

502

503 **Funding:** This work has been supported by the University of Ferrara via
504 FAR grants 2020 and 2021.

505 **References**

- 506 [1] Sekiguchi, Y., Sato, C. (2021) *Experimental investigation of the effects of*
507 *adhesive thickness on the fracture behavior of structural acrylic adhesive*
508 *joints under various loading rates*, Int. J. Adhes. Adhes., 105:102782.
- 509 [2] Miao, C., Fernandez, D., Heitzmann, M. T., Bailleres, H. (2019) *GFRP-*
510 *to-timber bonded joints: Adhesive selection*, Int. J. Adhes. Adhes., 94:29-
511 39.

- 512 [3] Yamamoto, A., Yoshida, T., Tsubota, K., Takamizawa, T., Kurokawa,
513 H., Miyazaki, M. (2006) *Orthodontic bracket bonding: enamel bond*
514 *strength vs time*, Am. J. Orthod. Dentofacial Orth., 130(4):435-e1.
- 515 [4] Benveniste, Y. and Miloh, T. (2001) *Imperfect soft and stiff interfaces*
516 *in two-dimensional elasticity*, Mech. Mat., 33 (6):309–323
- 517 [5] Hashin, Z. (2002) *Thin interphase/imperfect interface in elasticity with*
518 *application to coated fiber composites*, J. Mech. Phys. Solids, 50(12):2509–
519 2537.
- 520 [6] Frémond, M. (1987) *Adhesion of solids*, J. Mech. Theor. Appl., 6(3):383–
521 407.
- 522 [7] Bonetti E., Bonfanti G., Lebon F., Rizzoni, R. (2017) *A model of im-*
523 *perfect interface with damage*, Meccanica, 52(8):1911–1922
- 524 [8] Raous, M., Cangemi, L., Cocu, M. (1999) *A consistent model coupling*
525 *adhesion, friction, and unilateral contact*, Comput. Meth. Appl. Mech.
526 Eng., 177(3-4):383–399.
- 527 [9] Del Piero, G., Raous, M. (2010) *A unified model for adhesive interfaces*
528 *with damage, viscosity, and friction*, Eur. J. Mech.-A/Solid, 29(4):496–
529 507.
- 530 [10] Freddi, F., Frémond, M. (2006) *Damage in domains and interfaces: a*
531 *coupled predictive theory*, J. Mech. Mat. Struct., 1(7):1205-1233.
- 532 [11] Raffa, M.L., Lebon, F., Rizzoni R. (2016) *On modelling brick/mortar*

- 533 *interface via a St. Venant-Kirchhoff orthotropic soft interface. Part I:*
534 *theory*, Int. J. Masonry Res. Innov., 1 (2):142-164.
- 535 [12] Dumont, S., Lebon, F., Raffa, M. L., Rizzoni, R. (2017) *Towards nonlin-*
536 *ear imperfect interface models including micro-cracks and smeared rough-*
537 *ness*, Annal Solid Struct. Mech., 9(1-2):13–27.
- 538 [13] Raffa, M.L., Lebon, F., Rizzoni R. (2017) *On modelling crack/mortar*
539 *interface via a St. Venant-Kirchhoff orthotropic soft interface. Part II:*
540 *in silico analysis*, Int. J. Masonry Res. Innov., 2(4):259-273.
- 541 [14] Raffa, M. L., Lebon, F., Rizzoni, R. (2018) *Derivation of a model of im-*
542 *perfect interface with finite strains and damage by asymptotic techniques:*
543 *an application to masonry structures*, Meccanica, 53(7):1645-1660.
- 544 [15] Maurel-Pantel, A., Lamberti, M., Raffa M. L., Suarez, C., Ascione, F.,
545 Lebon, F. (2020) *Modelling of a GFRC adhesive connection by an imper-*
546 *fect soft interface model with initial damage*, Comp. Struct., 239:112034.
- 547 [16] Needleman, A. (1990) *An analysis of tensile decohesion along an inter-*
548 *face*, J. Mech. Phys. Solids, 38(3):289-324.
- 549 [17] Costanzo, F. (1998) *A continuum theory of cohesive zone models: defor-*
550 *mation and constitutive equations*, Int. J. Engng. Sci., 36(15):1763-1792.
- 551 [18] Alfano G., Sacco E. (2006) *Combining interface damage and friction in*
552 *a cohesive-zone model*, Int. J. Numer. Meth. Engng. 68 (5):542–582
- 553 [19] Chen, P., Chen, S., Peng, J. (2016) *Interface behavior of a thin-film*

- 554 *bonded to a graded layer coated elastic half-plane*, Int. J. Mech. Sci.
555 115:489-500.
- 556 [20] Chen, P., Peng, J., Chen, Z., Peng, G. (2019) *On the interfacial behavior*
557 *of a piezoelectric actuator bonded to a homogeneous half plane with an*
558 *arbitrarily varying graded coating*, Eng. Fract. Mech. 220:106627
- 559 [21] Guo, W., Chen, P., Yu, L., Peng, G., Zhao, Y., Gao, F. (2020) *Numerical*
560 *analysis of the strength and interfacial behaviour of adhesively bonded*
561 *joints with varying bondline thicknesses*, Int. J. Adhes. Adhes. 98:102553.
- 562 [22] Chen, P., Chen, S., Liu, H., Peng, J., Gao, F. (2020) *The interface behav-*
563 *ior of multiple piezoelectric films attaching to a finite-thickness gradient*
564 *substrate* J. Appl. Mech.-Trans. ASME, 87(1):041003.
- 565 [23] Lebon, F., Rizzoni, R. (2010) *Asymptotic analysis of a thin interface:*
566 *The case involving similar rigidity*, Int. J. Engng. Sci., 48:473–486
- 567 [24] Lebon, F., Rizzoni, R. (2011) *Asymptotic behavior of a hard thin linear*
568 *elastic interphase: An energy approach*, Int. J. Solid Struct., 48:441–449
- 569 [25] Rizzoni, R., Dumont, S., Lebon, F., Sacco, S. (2014) *Higher order model*
570 *for soft and hard interfaces*, Int. J. Solid Struct., 51:4137-4148
- 571 [26] Dumont, S., Rizzoni, R., Lebon, F., Sacco, E. (2018) *Soft and hard*
572 *interface models for bonded elements*, Comp. Part B: Engng., 153:480–
573 490.
- 574 [27] Furtsev, A., Lebon, E. (2020) *Variational approach to modelling soft*

- 575 *and stiff interfaces in the Kirchhoff-Love theory of plates*, Int. J. Solid
576 Struct., 202:562–574.
- 577 [28] Rudoy, E., Shcherbakov, V. (2020) *First-order shape derivative of the*
578 *energy for elastic plates with rigid inclusions and interfacial cracks*, Appl.
579 Math. Optim., 1-28.
- 580 [29] Baranova, S., Mogilevskaya, S. G., Nguyen, T. H., Schilling, D. (2020)
581 *Higher-order imperfect interface modelling via complex variables based*
582 *asymptotic analysis*, Int. J. Engng. Sci., 157:103390.
- 583 [30] Raffa, M.L., Lebon, F., Vairo, G. (2016) *Normal and tangential stiff-*
584 *nesses of rough surfaces in contact via an imperfect interface model*, Int.
585 J. Solid Struct., 87:245-253.
- 586 [31] Raffa, M. L., Rizzoni, R., Lebon, F. (2021) *A Model of Damage for Brit-*
587 *tle and Ductile Adhesives in Glued Butt Joints*, Technologies, 9(1):19.
- 588 [32] Kachanov, M., (1994) *Elastic solids with many cracks and related prob-*
589 *lems*, Adv. Appl. Mech., 30:257–445.
- 590 [33] Mauge C., Kachanov M. (1994) *Effective elastic properties of an*
591 *anisotropic material with arbitrarily oriented interacting cracks*, J. Mech.
592 Phys. Solid, 42:561–574.
- 593 [34] Tsukrov, I., Kachanov M. (2000) *Effective moduli of an anisotropic*
594 *material with elliptical holes of arbitrary orientational distribution*, Int.
595 J. Solid Struct., 37 (41):5919-5941.

- 596 [35] Kachanov, M., Sevostianov, I. (2005) *On quantitative characterization of*
597 *microstructures and effective properties*, Int. J. Solid Struct., 42(2):309-
598 336.
- 599 [36] Sevostianov, I., Kachanov, M. (2014) *On some controversial issues in*
600 *effective field approaches to the problem of the overall elastic properties*,
601 Mech. Mat., 69:93-105.
- 602 [37] Kachanov, M., Sevostianov, I. (2018) *Micromechanics of materials, with*
603 *applications*, (Vol. 249), Cham: Springer.
- 604 [38] Bruno, G., Kachanov, M., Sevostianov, I., Shyam, A. (2019) *Microme-*
605 *chanical modelling of non-linear stress-strain behavior of polycrystalline*
606 *microcracked materials under tension*, Acta Materialia, 164:50-59.
- 607 [39] Andrieux, S., Bamberger, Y., Marigo, J. J. (1986) *Un modèle de*
608 *matériau microfissuré pour les bétons et les roches*, J. Méc. Théor. Appl,
609 5(3)47:1-513.
- 610 [40] Welemane, H., Goidescu, C. (2010) *Isotropic brittle damage and unilat-*
611 *eral effect*, Compte Rendu Mec, 338(5):271-276.
- 612 [41] Sanchez-Palencia, E. (1992) *Non homogeneous materials and vibration*
613 *theory*, Lecture Notes in Physics, Springer, Berlin, 127.
- 614 [42] Hubert, J. S., Palencia, E. S. (1992) *Introduction aux méthodes asymp-*
615 *totiques et à l'hétérogénéisation: application à la mécanique des milieux*
616 *continus*, Masson.

- 617 [43] Klarbring A. (1991) *Derivation of the adhesively bonded joints by the*
618 *asymptotic expansion method*, Int. J. Engng. Sci., 29:493–512.
- 619 [44] Geymonat, G., Krasucki, F., Lenci, S. (1999) *Mathematical analysis of*
620 *a bonded joint with a soft thin adhesive*, Math. Mech. Solid, 16:201–215.
- 621 [45] Schmidt, P. (2008) *Modelling of adhesively bonded joints by an asymptotic*
622 *method*, Int. J. Engng. Sci., 46(12):1291-1324.
- 623 [46] Ciarlet P.G. (1988) *Mathematical Elasticity. Volume I: Three-*
624 *Dimensional Elasticity*, North-Holland, Amsterdam.
- 625 [47] Serpilli, M., Lenci, S. (2008) *Limit models in the analysis of three dif-*
626 *ferent layered elastic strips*, Eur. J.Mech.-A/Solids, 27(2):247-268.
- 627 [48] Serpilli, M., Lenci, S. (2016) *An overview of different asymptotic models*
628 *for anisotropic three-layer plates with soft adhesive*, Int. J. Solid Struct.,
629 81:130-140.
- 630 [49] Goidescu, C., Welemene, H., Karama, M., Gruescu, C. (2013) *Microcracks*
631 *closure effects in initially orthotropic materials*, Eur. J.Mech.-A/Solid,
632 37:172-184.
- 633 [50] Goidescu, C., Welemene, H., Pantalé, O., Karama, M., Kondo,
634 D. (2015) *Anisotropic unilateral damage with initial orthotropy: A*
635 *micromechanics-based approach*, Int. J. Damage Mech., 24(3):313-337.
- 636 [51] Eshelby, J. D. (1961) *Progress in solid mechanics*, J. Mech. Phys. Solid,
637 9(1):67-67.

- 638 [52] Welemane, H., Cormery, F. (2002) *Some remarks on the damage unilat-*
639 *eral effect modelling for microcracked materials*, Int. J. Damage Mech.,
640 11(1):65-86.
- 641 [53] Frémond, M., Nedjar, B. (1996) *Damage, gradient of damage and princi-*
642 *ple of virtual power*, Int. J. Solid Struct., 33(8):1083-1103.
- 643 [54] Chaboche, J. L. (1988) *Continuum damage mechanics: Part I—General*
644 *concepts*, J. Appl. Mech., 55:59-64.
- 645 [55] Wolfram Research, Inc. *Mathematica*; Version 12.2; Wolfram Research,
646 Inc.: Champaign, IL, USA, 2020.
- 647 [56] Murakami, S., Sekiguchi, Y., Sato, C., Yokoyama, E., Furusawa, T. (2016)
648 *Strength of cylindrical butt joints bonded with epoxy adhesives under*
649 *combined static or high-rate loading*, Int. J. Adhes. Adhes., 67:86–93.